Araştırma Makalesi/Research Article
https://doi.org/10.51489/tuzal.1395189

2024; 6(1); 12-25

Turkish Journal of Remote Sensing

https://dergipark.org.tr/en/pub/tuzal

e-ISSN 2687-4997

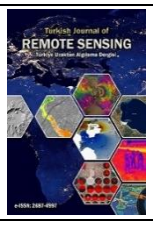

Determination of the Effects of Various Spectral Index Combinations on Seasonal Land Use and Land Cover (LULC) Changes Using Random Forest (RF) Classification Case Study: Southeast Marmara Region 2016-2020

Eda Aşci[1], Levent Genç[*2,3]

[1]*Çanakkale Onsekiz Mart University, Engineering Faculty, Geomatics Engineering, Çanakkale, Turkey*
[2]*Çanakkale Onsekiz Mart University, Faculty of Architecture and Design, Department of Urban and Regional Planning, Land Use and Climate Change Laboratory, Çanakkale, Turkey*
[3]*Canakkale Onsekiz Mart University, Computer-Agriculture-Planning (ComAgPlan) Study Group, Canakkale, Turkey*

Keywords
Remote Sensing
LULC
Vegetation Indices
South-Eastern Marmara Region

ABSTRACT

The effects of irregular population growth, migration mobility, and vegetation dynamics by humans can lead to changes in Land Use and Land Cover (LULC). Changes in LULC are particularly significant in coastal areas associated with industrial activities. The southeastern Marmara region, which is one of Turkey's industrial coastal areas, is also affected by the surrounding changes. The study area was selected to determine LULC change and classification accuracy using Sentinel-2 vegetation indices combinations. In the study area, the Gemlik-Bursa Northern Interchange Investments Area and TOGG (Turkey's Automobile Initiative Group) factory are located. The study area was determined by creating a 5-km buffer zone from the coast to the mainland covering Armutlu district of Yalova province and Osmangazi, Mudanya, and Gemlik districts of Bursa province. Random Forest (RF) classification technique was applied both to the original bands and to 21 new band combinations that are derived from Sentinel-2 multispectral satellite imagery for 3 seasons in 2016 and 2020. The new band combinations used for classification were created by adding the normalized vegetation indices, the original bands and the bands obtained from the simple ratio formula. In 2016, the highest accuracy results for the winter, spring, and summer seasons were observed for the OI12 (82.93%), ORF (84.44%), and ORF (84.67%) indices, while in 2020 were observed for the OI5 (85.89%), ORF (84.75%), and OI6 (84.63%) indices. In Southeast Marmara, investment decisions taken at national level have led to population growth in the region. Although it was observed that there was no significant change in classification accuracy with the addition of spectral features to the original bands such as NDVI and SR, we believe that future testing of the data with different statistical and machine learning methods provide higher accuracy.

Spektral İndeks Kombinasyonlarının Rastgele Orman (RO) Sınıflandırması Kullanarak Mevsimsel Arazi Kullanımı ve Bitki Örtüsü (AKBÖ) Değişiklikleri Üzerindeki Etkilerinin Belirlenmesi: Güneydoğu Marmara Bölgesi Örneği 2016-2020

Anahtar Kelimeler:
Uzaktan Algılama
AKBÖ
Vejetasyon İndeksler
Güney-Doğu Marmara Bölgesi

ÖZ

Düzensiz nüfus artışı, göç hareketliliği ve insanların vejetasyon dinamiklerine etkileri Arazi Kullanım ve Bitki Örtüsü (AKBÖ) değişimlerine yol açabilmektedir. AKBÖ değişiklikleri sanayi ile ilişkili kıyı bölgelerinde oldukça önemlidir. Türkiye'nin önemli kıyı alanlarından olan Güneydoğu Marmara alanı da çevredeki değişimlerden etkilenmektedir. Çalışma alanı, Sentinel-2 tabanlı bitki örtüsü indeksleri kombinasyonlarını kullanarak gerek AKBÖ değişimini gerekse sınıflandırmanın doğruluğunu belirlemek amacıyla seçilmiştir. Çalışma alanında Gemlik- Bursa Kuzey Kavşağı yatırım alanı ve yeni inşa edilen TOGG (Türkiye'nin Otomobili Girişim Grubu) fabrikası yer almaktadır. Çalışma alanı, Yalova ili Armutlu ilçesi ve Bursa ili Osmangazi, Mudanya ve Gemlik ilçelerini kapsayan alanda kıyıdan anakaraya 5 km'lik tampon bölge

Article Info

Received: 23/11/2023
Accepted: 21/01/2024
Published: 30/06/2024

Citation:

Aşci, E. & Genç, L. (2024). Determination of the Effects of Various Spectral Index Combinations on Seasonal Land Use and Land Cover (LuLc) Changes Using Random Forest (RF) Classification Case Study: Southeast Marmara Region 2016-2020. Turkish Journal of Remote Sensing, 6 (1), 12-25.

***Corresponding Author:** Levent Genc, leventgc@comu.edu.tr, +90 286 218 0018 (3032)

oluşturularak belirlenmiştir. Rastgele Orman (RO) sınıflandırma tekniği, 2016 ve 2020 yıllarında 3 sezon boyunca Sentinel-2 multispektral uydu görüntülerinden elde edilen indeksler kullanılarak orijinal bantlara ve 21 yeni bant kombinasyonuna uygulanmıştır. Sınıflandırma için kullanılan yeni bant kombinasyonları, normalize edilmiş bitki örtüsü indeksleri (NDVI), orijinal bantlar ve basit oran (SR) formülünden elde edilen bantlar eklenerek oluşturulmuştur. En yüksek doğruluk sonuçları 2016 yılı kış, ilkbahar ve yaz mevsimleri için OI12 (%82,93), ORF (%84,44) ve yine ORF (%84,67) indekslerinde gözlemlenirken, 2020 yılında OI5 (%85,89), ORF (%84,75) ve OI6 (%84,63) indekslerinde gözlemlenmiştir. Güneydoğu Marmara'da ulusal düzeyde alınan yatırım kararları bölgede nüfus artışına yol açmıştır. NDVI ve SR gibi orijinal bantlara spektral özelliklerin eklenmesiyle sınıflandırma doğruluğunda önemli bir değişiklik olmadığı gözlemlenmiş olsa da verilerin gelecekte farklı istatistiksel ve makine öğrenimi yöntemleriyle test edilmesinin sınıflama doğruluğunu daha fazla artırabilir.

1. INTRODUCTION

Land use and land cover (LULC) dynamics and understanding their relationship with the environment are important. It is known that LULC occur due to natural or human-induced events (Dewidar, 2010). Changes in LULC at regional and global level can be associated with irregular migration movements, population changes, industrial developments, agricultural activities, and forest fires. Therefore, understanding these changes is of great importance, especially in identifying the pressure caused by impervious surfaces. The investigation of land cover changes through quantitative data analysis and visual interpretation is possible through Remote Sensing (RS). Many researchers have preferred to use RS data to reveal the results of land cover change (El-naggar, 2018; Joshi et al., 2011; Sharma & Joshi, 2016). RS data is commonly used in geographic information production due to its ability to provide data at different resolutions according to land conditions, as well as its open-access and free availability. The Sentinel data, provided by the European Space Agency (ESA), are one of the sources contributing to the production of high-quality information since 2015 (Cavur et al., 2019; Myint Htun et al., 2023; Yulianti, 2019). RS data is widely used, especially in determining the reasons for changes in urban areas, studying spatial changes in vegetation classes, and investigating the impact of different resolution bands on the land, etc. It is known that the spatial changes in cities are associated with industrial investments and population changes, and this uncontrolled progression is thought to influence LULC and urban planning. Studies highlight the pressure on urban dynamics caused by development decisions, especially in industrial areas (Batunacun et al., 2018; Chandra Pandey et al., 2019). Additionally, it is observed that satellite data, with their band combinations, can be used to examine these changes and developments, yielding more realistic results in various land cover classes.

In this context, different methods and techniques that emerge for determining LULC changes are considered sustainable in terms of facilitating scientific research. When determining LULC change results, classification techniques and different band combinations suitable for the study areas are commonly used. Many researchers strive to achieve maximum accuracy in LULC classification through mathematical and statistical inferences. Machine Learning (ML) algorithm is one of them. An ML algorithm such as Random Forest (RF) is frequently used when monitoring LULC changes in urban land cover and vegetation classification (Asci et al., 2021; Breiman, 2001; Chehata et al., 2009; Scornet, 2015). The RF technique is used to separate pixels based on their spectral values. It involves assigning the training data's previously learned information to LULC classes. With its tree structure, it aims to minimize the error between pixels, thus enhancing accuracy in classification (Guan et al., 2012). Another method aimed at improving classification accuracy involves creating new band combinations (Genc, 2002). This allows for the identification of changes on the ground by understanding how pixels with dominant spectral reflectance values respond to new band combinations.

Learning the change dynamics of LULC classes through satellite data enables easier and more appropriate development of sustainable projects. RS has been used extensively to track developments, especially in industrial areas, to link local knowledge with global outcomes, and to explore new analyses and mathematical expressions for understanding the landscape. (Mukhawana et al., 2023; Sathian & Brema, 2023). It is important to calculate the accuracy of the classifications made in different ways as an indicator and learn about the feasibility of using this method (Kumar & Agrawal, 2019). We can use these results.

Bursa and Yalova provinces in Turkey are positioned within the category of developing and rapidly growing regions, often referred to as industrial cities. While the rapid developments in the industrial sector impact various aspects of life, their contributions to the country's Gross Domestic Product (GDP) may change. Factors such as significant investment decisions have led to an acceleration in migration activities and irregular population growth in industrial-focused regions.

In this context, Bursa, which is known as an industrial city in Turkey and where projects such as 'Turkey's Automobile Joint Venture Group' (TOGG) and Bursa-North Interchange are located, was

selected as the coastal study area together with Yalova province.

The aim of the study is to determine the accuracy performance of the images created with combinations of indices produced using Sentinel-2A satellite data. Secondary aims include examining the LULC changes that occurred during the construction of the government - supported TOGG factory in the area.

2. MATERIALS and METHOD

2.1. Study Area

The study area consists of the Gemlik district of Bursa, with 13 neighborhoods; the Mudanya district of Bursa with 17 neighborhoods; 2 neighborhoods in the Osmangazi district of Bursa; and 7 villages in the Armutlu district of Yalova province, covering a total area of 495,864 km^2 in the southeast of the Marmara region in Turkey (Figure 1). As the province of Yalova has a different form of administration, the term 'village' is used instead of 'neighborhood'.

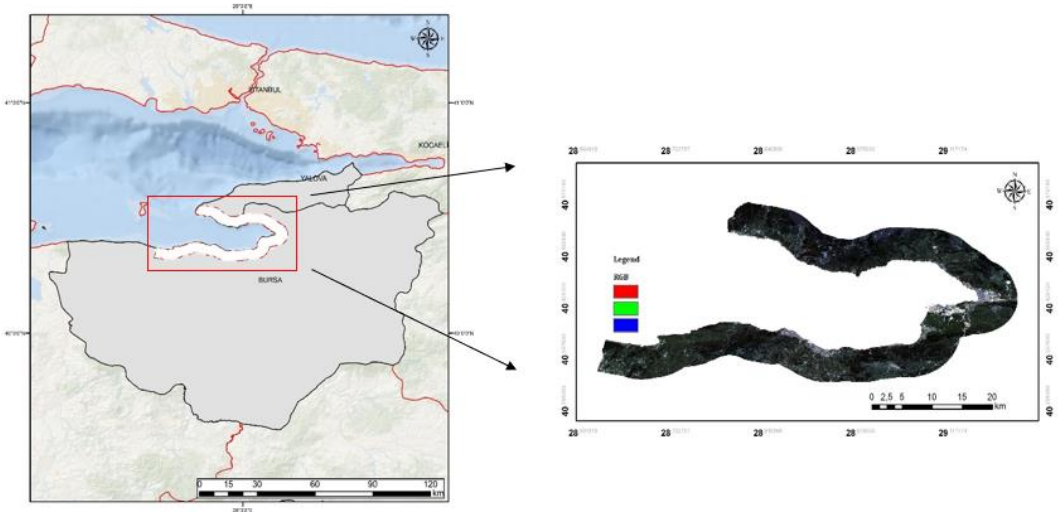

Figure 1. Study area

The study area has been defined by selecting a 5-km buffer zone from the coastline towards the mainland. The complete list of villages and neighborhoods in the area is given in Table 1.

Table 1. List of neighborhoods and villages in study area

City	District	Neighborhood Village
Bursa	Gemlik	Cihatlı Neighborhood Engurucuk Neighborhood Karacaali Neighborhood Kurtul Neighborhood Kucukkumla Neighborhood Narli Neighborhood Yenikoy Neighborhood Ata Neighborhood Buyukkumla Neighborhood Gencali Neighborhood Kumla Neighborhood Kursunlu Neighborhood Parsbey Neighborhood
Bursa	Osmangazi	Osmangazi Neighborhood Gundogdu Neighborhood
Bursa	Mudanya	Altintas Neighborhood Aydinpinar Neighborhood Burgaz Neighborhood Camlik Neighborhood Cepni Neighborhood Egerce Neighborhood Esence Neighborhood Goynuklu Neighborhood Haitpasa Neighborhood Isıklı Neighborhood Kumkaya Neighborhood Mesudiye Neighborhood Sogutpinar Neighborhood Tirilye Neighborhood

		Yali Neighborhood

Table 1. Cont.

City	District	Neighborhood Village
Bursa	Mudanya	Yaliciftlik Neighborhood Yaman Neighborhood Yorukali Neighborhood
Yalova	Armutlu	Hayriye Village Fistikli Village Kapakli Village Mecidiye Village Bayir Neighborhood Karsiyaka Neighborhood 50. Yil Neighborhood

2.2. Data Used

The Sentinel-2 mission is a terrain monitoring mission consisting of two satellites (Sentinel-2a and Sentinel-2b) providing optical imagery in 13 spectral bands. It has a spatial resolution ranging from 10 m to 60 m (Table 2).

The study obtained six Sentinel-2A satellite images for the years 2016 and 2020 from the European Space Agency Copernicus website (https://scihub.copernicus.eu/). Image processes were applied to the images taken on January 9, 2016, April 18, 2016, August 16, 2016, February 2, 2020, April 17, 2020, and August 15, 2020.

Table 2. Sentinel – 2 bands features

Sentinel-2 Bands	Central Wavelength(µm)	Resolution (m)
Band 1 – Coastal Aerosol	0.443	60 m
Band 2 – Blue	0.492	10 m
Band 3 – Green	0.560	10 m
Band 4 – Red	0.665	10 m
Band 5 – Vegetation Red Egde	0.704	20 m
Band 6 – Vegetation Red Egde	0.741	20 m
Band 7 – Vegetation Red Egde	0.783	20 m
Band 8 – NIR	0.833	10 m
Band 8a – Vegetation Red Egde	0.865	20 m
Band 9 – Water Vapour	0.945	60 m
Band 10 – SWIR – Cirrus	0.1374	60 m
Band 11 – SWIR	0.1614	20 m
Band 12 – SWIR	0.2202	20 m

2.3. Pre-Preprocessing and Classification

The satellite images to be used in the study may contain various errors. To make the images usable by rectifying errors, pre-processing has been applied to the images. The Sentinel-2A satellite data used in the study are Level 1 data, which have not undergone atmospheric correction. Therefore, an atmospheric correction process was applied to the images initially. Subsequently, a reprojection process was applied to bring the images into convenient projection. A resampling process was carried out to ensure that the bands with different resolutions in the satellite image have a consistent resolution (all at 10 m). All images were determined by considering a 5-km buffer zone and then clipped from the main image. All processing steps were carried out using the SNAP 7.0 program.

The preferred method in this research is shaped by extracting prominent features in images using spectral indices and then classifying all generated images with the RF classification technique to create LULC maps (Chan & Paelinckx, 2008; Ghimire et al., 2010; Pal, 2005).

The classification process has been created with six LULC classes: Agriculture (A), Forest (F), Olive (O), Pasture (P), Urban (U), and Water (W). In the selection of these classes, fieldwork was conducted to detect LULC types, and the classes were determined through visual interpretation. A total of 2050 training data were used for classification for the 6 LULC classes. For accuracy analysis, 410 ground control points were randomly selected for each classification to form homogeneous test data for the 6 LULC classes (training/test data: 2050/410). The process from acquiring the images to the accuracy analysis is shown in Figure 2.

Figure2. Flowchart of the study

Image classification is commonly used in RS to obtain quantitative data from satellite images (Baeza & Paruelo, 2020; Radhika & Varadar, 2016; Meinel & Neubert, 2004; Mendoza & Martins, 2006). In this study, a total of 2050 training vectors were defined for classification, with attention to the areas covered by the 6 LULC classes in the field. Information about the band combinations used in the classification process, as well as the names, formulas, and references to the resulting indices, can be found in Table 3. In the nomenclature of the combinations in Table 3, 'O' represents the original bands (10 bands) in the image, 'I' represents the new band created with the NDVI index (Table 3), and 'SR' represents the new band created with the simple ratios (Table 3).

Table 3. Indices and their features

Name	Bands	Formula	Classification Method	Algorithm	References
O_{RF}	B2, B3, B4, B5, B6, B7, B8, B8A, B11, B12	*B2+B3+B4+B5+ B6+B7+B8+B8A+B 11+B12*	Random Forest	Machine Learning	(Colkesen et al., 2021; Demarchi, et al., 2014; Goel & Abhilasha, 2017; Hütt et al., 2016; Jamali & Abdul Rahman, 2019a, 2019b; Kavzoglu et al., 2015; Phiri et al., 2020; Rodriguez-Galiano et al., 2012; Wu et al., 2021)
OI_5	B2, B3, B4, B6, B7, B8, B8A, B11, B12	$B2+B3+B4+B6+ B7+B8+B8A+B11+ B12+(\frac{B5-B4}{B5+B4})$	Random Forest	Machine Learning	(Ahamed et al., 2011; Gitelson et al., 2002)
OI_6	B2, B3, B4, B5, B7, B8, B8A, B11, B12	$B2+B3+B4+B5+ B7+B8+B8A+B11+ B12+(\frac{B6-B4}{B6+B4})$	Random Forest	Machine Learning	(Xianju et al., 2017)
OI_7	B2, B3, B4, B5, B6, B8, B8A, B11, B12	$B2+B3+B4+B5+ B6+B8+B8A+B11+ B12+(\frac{B7-B4}{B7+B4})$	Random Forest	Machine Learning	(Zarco-Tejada et al., 2001)
OI_8	B2, B3, B4, B5, B6, B7, B8A, B11, B12	$B2+B3+B4+B5+ B6+B7+B8A+B11+ B12+(\frac{B8-B4}{B8+B4})$	Random Forest	Machine Learning	(Barnes et al., 2000; Herrmann et al., 2011; Le Maire et al.,2004; Main et al., 2011; Penuelas et al., 1997; Wu et al., 2008)
OI_{8a}	B2, B3, B4, B5, B6, B7, B8, B11, B12	$B2+B3+B4+B5+ B6+B7+B8+B11+B 12+(\frac{B8A-B4}{B8A+B4})$	Random Forest	Machine Learning	(Tesfaye et al., 2021 Tucker, 1980; Zhang et al., 2017)
OI_{11}	B2, B3, B4, B5, B6, B7, B8, B8A, B12	$B2+B3+B4+B5+ B6+B7+B8+B8A+B 12+(\frac{B11-B4}{B11+B4})$	Random Forest	Machine Learning	Panigrahy et al., 2009; Tucker, 1979)
OI_{12}	B2, B3, B4, B5, B6, B7, B8, B8A, B11	$B2+B3+B4+B5+ B6+B7+B8+B8A+B 11+.(\frac{B12-B4}{B12+B4})$	Random Forest	Machine Learning	-
OI_5SR_6	B2, B3, B4, B7, B8, B8A, B11, B12	$B2+B3+B4+B7+ B8+B8A+ B11+B12+ (\frac{B5-B4}{B5+B4})+(\frac{B6}{B5})$	Random Forest	Machine Learning	-
OI_5SR_7	B2, B3, B4, B6, B8, B8A, B11, B12	$B2+B3+B4+B6+ B8+B8A+ B11+B12+ (\frac{B5-B4}{B5+B4})+(\frac{B7}{B5})$	Random Forest	Machine Learning	-

Table 3. Cont.

Name	Bands	Formula	Classification Method	Algorithm	References
OI_6SR_6	B2, B3, B4, B7, B8, B8A, B11, B12	B2+B3+B4+B7+ B8+B8A+ B11+B12+ $(\frac{B6-B4}{B6+B4})+(\frac{B6}{B5})$	Random Forest	Machine Learning	-
OI_6SR_7	B2, B3, B4, B8, B8A, B11, B12	B2+B3+B4+ B8+B8A+ B11+B12+ $(\frac{B6-B4}{B6+B4})+(\frac{B7}{B5})$	Random Forest	Machine Learning	-
OI_7SR_6	B2, B3, B4, B8, B8A, B11, B12	B2+B3+B4+ B8+B8A+ B11+B12+ $(\frac{B7-B4}{B7+B4})+(\frac{B6}{B5})$	Random Forest	Machine Learning	-
OI_7SR_7	B2, B3, B4, B6, B8, B8A, B11, B12	B2+B3+B4+ B6+B8+B8A+ B11+B12+ $(\frac{B7-B4}{B7+B4})+(\frac{B7}{B5})$	Random Forest	Machine Learning	-
OI_8SR_6	B2, B3, B4, B7, B8A, B11, B12	B2+B3+B4+ B7+ B8A+ B11+B12+ $(\frac{B8-B4}{B8+B4})+(\frac{B6}{B5})$	Random Forest	Machine Learning	-
OI_8SR_7	B2, B3, B4, B6, B8A, B11, B12	B2+B3+B4+ B6+ B8+B8A+ B11+B12+ $(\frac{B8-B4}{B8+B4})+(\frac{B7}{B5})$	Random Forest	Machine Learning	-
$OI_{8a}SR_6$	B2, B3, B4, B7, B8, B11, B12	B2+B3+B4+ B7+ B8+ B11+B12+ $(\frac{B8A-B4}{B8A+B4})+(\frac{B6}{B5})$	Random Forest	Machine Learning	-
$OI_{8a}SR_7$	B2, B3, B4, B6, B8, B11, B12	B2+B3+B4+ B6+ B8+ B11+B12+ $(\frac{B8A-B4}{B8A+B4})+(\frac{B7}{B5})$	Random Forest	Machine Learning	-
$OI_{11}SR_7$	B2, B3, B4, B6, B8, B8A, B12	B2+B3+B4+ B6+ B8+B8A+ B12+ $(\frac{B11-B4}{B11+B4})+(\frac{B7}{B5})$	Random Forest	Machine Learning	-
$OI_{12}SR_6$	B2, B3, B4, B7, B8, B8A, B11	B2+B3+B4+ B7+ B8+B8A+ B11+ $(\frac{B12-B4}{B12+B4})+(\frac{B6}{B5})$	Random Forest	Machine Learning	-
$OI_{12}SR_7$	B2, B3, B4, B6, B8, B8A, B11	B2+B3+B4+ B6+ B8+B8A+ B11 + $(\frac{B12-B4}{B12+B4})+(\frac{B7}{B5})$	Random Forest	Machine Learning	-

2.4. Classification

Indices are a mathematical set of operations frequently used in RS that enable the extraction of dominant features by utilizing spectral bands to understand the state of the terrain. The goal is to determine changes in LULC by examining the responses provided by the values in the bands for specific information extraction over an area. Various combinations are created to obtain the desired geographic information, resulting in the generation of indices.

A total of 21 indices have been created in the study. Seven of these indices contain only the bands formed in the 'I' shape, while the remaining 14 include bands formed in both 'I' and 'SR' shapes. The bands referred to as 'I' use NDVI mathematics, while the bands referred to as 'SR' use simple ratio mathematics. When creating these indices, all bands used in the new bands (except the red band - B4) have been subtracted from the original band content.

In this way, the subtracted original bands and the newly created index bands have been combined.

The RF classification technique involves constructing patterns by forming multiple decision trees with random input data, including a structural classification process (Perumal & Bhaskaran, 2010). Decision trees are created by branching test data in the training process (Goel & Abhilasha, 2017).

In this context, each tree is determined by combinations arising from the data in the field and the vectors affected by independent variables. Each input vector data contains pixel values within its content (Breiman, 2001; Phiri et al., 2020). When compared to other machine learning techniques, the reason for preferring RF is its ability to make pixel values meaningful with a small amount of training data and its high capability for fast processing.

RF classification technique uses the Gini index as a criterion in the machine learning algorithm. The equation for the Gini index is given in Equation 1 below. It is used as an attribute selection criterion to measure the impurity of a feature with respect to classes (Pal, 2005).

$$\sum\sum(fC_i,T)/(|T|)\ (fC_J,T)/(|T| \quad (1)$$

The Gini index branches the test data into a tree structure based on classes. Here, T represents the training dataset, and performs random pixel assignment is performed to the representative of class C_i (Pal, 2005).

2.5. Accuracy Assessment

Accuracy analysis is crucial in UA (Akturk & Altunel, 2019; Whiteside et al., 2011) for quantifying the accuracy of classification outputs on a class-by-class basis. It is important for investigating discrepancies between satellite data and actual terrain and examining user errors. In the verification process, the comparison between each pixel in the field and ground control points is used to understand the quality of the generated data.

In the study, control points were randomly selected homogeneously from different pixels considering the areas of LULC classes. Accuracy analysis conducted total 410 ground control points were created in the Google Earth Pro program for the 6 main LULC classes in each classification. According to the equation found in Guan et al. (2012), ground control points were selected beyond the maximum number for each class for the verification process (Equations 2). For the accuracy analysis of the classification, ground sample points were obtained separately for each classification, with a total of 410 homogenous points for each classification. The created ground control points were processed on Sentinel-2 satellite imagery with 10 m resolution. The indices that yielded the highest and lowest accuracy as a result of the combinations were determined separately for each of the three seasons. The equations used to create the error matrix in the study are provided in Equations 3 and 4 (Zaidi et al., 2017). Accuracy assessment results in the classified images were obtained for the RF classification technique using SNAP 7.0 software.

$$N = \frac{Z^2 * p(100-q)}{E^2} \quad (2)$$

N = number of points to be selected
Z = two-sided confidence level (from normal standard deviation)
p = expected percentage accuracy
q = logic operator
E= allowable error

$$Overall\ Accuracy = \frac{Sum\ of\ true\ random\ points}{Cumulative\ sum\ of\ all\ random\ points} \quad (3)$$

$$k_c = \frac{Observed - Expected}{1 - Expected} \quad (4)$$

3. RESULTS

In this study, which explored new created index combinations, the aim was to find the combination that provides the highest accuracy in classification.

3.1. Results of the Accuracy Analysis of the LULC Classification

In all accuracy analysis results, the highest and lowest accuracy rates for the years 2016 and 2020 are as follows for different seasons.

For the 2016-winter season (OI_8SR_7- overall accuracy: 76.04%, kappa: 0.73, OI_{12}- 82.93%, 0. 79), for the 2016-spring season ($OI_{11}SR_7$- 76.16%, 0.71, O_{RF}-84.44%, 0.82), 2016-summer season (OI_{8a}- 76.64%, 0.71, O_{RF}- 84.67%, 0. 83%) and respectively, 2020-winter season ($OI_{11}SR_7$- overall accuracy: 75.12%, kappa: 0.70, O_{RF}- 82.72%, 0.79), 2020-spring season ($OI_{12}SR_7$- 75. 12, 0.70%, O_{RF}- 84.75%, 0.82), for 2020-summer season ($OI_{11}SR_7$- 78.05%, 0.73, O_{I6}- 84.63%, 0.81) (Table 4-Table 5).

The results of the accuracy analysis conducted for RF classification using original satellite image bands and classification with a combination of 21 indices, in terms of the reasons for the highest and lowest accuracy, are as follows:

- For the winter season of 2016, classification results have been obtained for OI_{12} (high) and OI_8SR_7 (low) (Table 4). OI_{12} yielded a high classification result because, during the period when Band 12 had an impact, there was a high moisture content in the early growth stage of crops in the study area. Additionally, the specific characteristics of the index used in its mathematics, such as B12 measuring moisture content (for both soil and vegetation) and B8 being used for vegetation detection, contributed to the high result. In the classification of OI_8SR_7, it was observed that on the specified date, the mathematical expression did not capture the

vegetation pixels with Band 8 (B8). Band 7 (B7) did not have an impact on pixel visibility because it was subtracted from the original bands.

- For the spring season of 2016 (Table 4), the O_{RF} classification provided better discrimination for both urban and agricultural areas. This was attributed to the fact that the original content and combination of the ten bands remained unchanged. At the examined date, the land surface was covered with vegetation up to 70-80%, facilitating the distinction between urban and agricultural areas. Similarly, in the $OI_{11}SR_7$ classification for the same season, the low accuracy rate was exclusion of Band 5 (B5) and B7 from the original band combination. Attributed to the weakening of detection due to the vegetation at the date (mostly in the early growth stage). This was also due to the challenge of detection caused by Band 11 (B11)'s wide band range.
- In the summer season of 2016 (Table 4), once again, the O_{RO} classification provided higher accuracy results for the same reasons as the spring season. However, it was believed that the low accuracy of the OI_{8a} index might have been due to the agricultural areas not being selected in the classification process because the vegetation cover in the study area was less extensive.

Table 4. Results of the Accuracy Analysis in 2016(light blue: low accuracy, pink: high accuracy

Bands	9.01.2016				18.04.2016				16.08.2016			
	Producer	User	Overall	Kappa	Producer	User	Overall	Kappa	Producer	User	Overall	Kappa
O_{RF}	0.839	0.788	81.220	0.769	0.800	0.711	84.436	0.815	0.619	0.963	84.670	0.826
OI_5	0.926	0.806	79.756	0.773	0.895	0.773	79.512	0.723	0.944	0.791	81.265	0.741
OI_5SR_6	0.740	0.673	76.832	0.721	0.840	0.778	78.537	0.744	0.760	0.844	78.586	0.744
OI_5SR_7	0.780	0.639	77.750	0.744	0.700	0.745	79.268	0.723	0.780	0.830	78.345	0.747
OI_6	0.854	0.854	82.439	0.734	0.880	0.786	77.995	0.688	0.833	0.811	79.756	0.769
OI_6SR_6	0.780	0.661	77.017	0.717	0.820	0.774	78.832	0.743	0.760	0.826	78.832	0.738
OI_6SR_7	0.780	0.661	78.780	0.720	0.680	0.756	77.129	0.717	0.740	0.822	78.838	0.735
OI_7	0.743	0.788	78.293	0.718	0.955	0.824	80.456	0.728	0.774	0.828	81.707	0.752
OI_7SR_6	0.780	0.672	76.585	0.721	0.860	0.782	78.780	0.739	0.800	0.833	78.345	0.741
OI_7SR_7	0.740	0.627	76.829	0.709	0.860	0.768	76.642	0.739	0.800	0.833	78.102	0.738
OI_8	0.737	0.737	77.317	0.748	0.974	0.804	77.805	0.740	0.875	0.718	79.512	0.764
OI_8SR_6	0.780	0.661	76.830	0.720	0.820	0.745	78.431	0.741	0.800	0.833	78.589	0.740
OI_8SR_7	0.820	0.661	76.039	0.731	0.860	0.768	78.378	0.749	0.780	0.830	78.398	0.738
OI_{8a}	0.828	0.857	76.755	0.708	0.750	0.818	76.341	0.710	0.862	0.543	76.642	0.710
$OI_{8a}SR_6$	0.780	0.672	77.017	0.722	0.840	0.750	78.780	0.744	0.780	0.830	78.208	0.736
$OI_{8a}SR_7$	0.780	0.672	76.773	0.719	0.880	0.786	79.024	0.746	0.860	0.827	79.707	0.755
OI_{11}	0.895	0.895	80.813	0.758	0.923	0.750	78.166	0.721	0.862	0.862	80.976	0.761
$OI_{11}SR_6$	0.780	0.661	76.284	0.714	0.760	0.679	76.341	0.714	0.800	0.816	78.832	0.744
$OI_{11}SR_7$	0.800	0.690	78.240	0.737	0.800	0.667	76.156	0.712	0.860	0.827	79.319	0.750
OI_{12}	0.931	0.844	82.927	0.791	0.766	0.818	76.341	0.708	0.750	0.871	80.244	0.755
$OI_{12}SR_6$	0.820	0.683	77.017	0.722	0.740	0.822	77.073	0.722	0.860	0.827	79.218	0.749
$OI_{12}SR_7$	0.828	0.857	76.286	0.716	0.860	0.811	78.398	0.739	0.840	0.824	79.075	0.747

- For the winter season of 2020, the OI_5 classification provided higher accuracy results (Table 5) because agricultural areas did not exhibit significant features at the examined date, while urban and other areas did. Furthermore, the absence of mathematical operations on the original ten bands contributed to the higher accuracy. In contrast, the $OI_{11}SR_7$ index was found to not match agricultural areas due to the bands included in its content, which did not allow for the measurement of moisture content and vegetation content.
- For the spring season of 2020 (Table 5), the significant effect of the O_{RF} index, like the spring season of 2016, was understood to be due to the same influencing factors. The low results of the $OI_{12}SR_7$ index can be attributed to the exclusion of B5 and B7 from the original bands, crucial for vegetation analysis. Additionally, along with the detection weakness in the combination formed with Band 12 (B12), provides an explanation for the observed low values.
- For the summer season of 2020 (Table 5), OI6 index was identified as more suitable for classification. This suitability stems from its interaction with the red-edge band in the original bands, thereby enhancing its discriminative power for vegetation separation, especially during the targeted season. On the other hand, for $OI_{11}SR_7$, it was understood that there were no products in the field where the moisture content in vegetation would have an effect, and the removal of B5 and B7 from the original bands had a negative impact.

Table 5. Results of the Accuracy Analysis in 2020 (light blue: low accuracy, pink: high accuracy)

Bands	2.02.2020				17.04.2020				15.08.2020			
	Producer	User	Overall	Kappa	Producer	User	Overall	Kappa	Producer	User	Overall	Kappa
O_{RF}	0.925	0.803	82.716	0.788	0.828	0.649	84.748	0.817	0.926	0.806	82.439	0.785
OI_5	0.838	0.775	85.885	0.790	0.920	0.742	83.659	0.798	0.864	0.905	81.944	0.813
OI_5SR_6	0.821	0.657	79.756	0.756	0.844	0.864	78.802	0.795	0.700	0.972	81.220	0.792
OI_5SR_7	0.893	0.610	78.293	0.761	0.857	0.706	75.610	0.739	0.780	0.800	80.244	0.808
OI_6	0.829	0.850	82.683	0.701	0.935	0.906	84.185	0.783	0.743	0.788	84.634	0.770
OI_6SR_6	0.700	0.778	79.756	0.720	0.844	0.809	82.927	0.757	0.829	0.806	82.809	0.744
OI_6SR_7	0.720	0.766	80.244	0.732	0.778	0.833	78.537	0.728	0.786	0.733	84.146	0.763
OI_7	0.870	0.930	76.039	0.739	0.853	0.906	82.816	0.741	0.710	0.815	81.573	0.746
OI_7SR_6	0.700	0.745	76.829	0.711	0.857	0.706	79.756	0.749	0.600	0.844	78.922	0.768
OI_7SR_7	0.821	0.657	77.805	0.743	0.857	0.667	77.317	0.748	0.867	0.765	80.488	0.783
OI_8	0.957	0.898	79.024	0.748	0.813	0.830	79.951	0.800	0.750	0.828	79.024	0.779
OI_8SR_6	0.683	0.778	76.098	0.757	0.800	0.783	79.024	0.749	0.800	0.833	80.779	0.772
OI_8SR_7	0.683	0.757	78.780	0.739	0.711	0.762	78.810	0.708	0.780	0.848	81.951	0.760
OI_{8a}	0.773	0.895	76.098	0.706	0.964	0.871	79.661	0.739	0.778	0.778	81.220	0.768
$OI_{8a}SR_6$	0.700	0.778	78.049	0.734	0.667	0.833	79.024	0.747	0.756	0.861	83.659	0.803
$OI_{8a}SR_7$	0.700	0.745	76.341	0.714	0.857	0.615	78.537	0.740	0.720	0.837	79.692	0.758
OI_{11}	0.879	0.967	76.456	0.698	0.882	0.833	77.805	0.714	0.829	0.853	82.022	0.774
$OI_{11}SR_6$	0.720	0.783	78.537	0.741	0.893	0.595	78.049	0.738	0.740	0.822	78.729	0.743
$OI_{11}SR_7$	0.700	0.700	75.122	0.700	0.756	0.756	75.610	0.708	0.740	0.787	78.049	0.734
OI_{12}	0.828	0.857	78.049	0.729	0.867	0.963	80.244	0.748	0.771	0.659	79.775	0.746
$OI_{12}SR_6$	0.740	0.771	76.585	0.717	0.857	0.686	79.268	0.750	0.740	0.804	78.832	0.744
$OI_{12}SR_7$	0.740	0.771	76.575	0.716	0.733	0.767	75.122	0.702	0.680	0.773	78.537	0.740

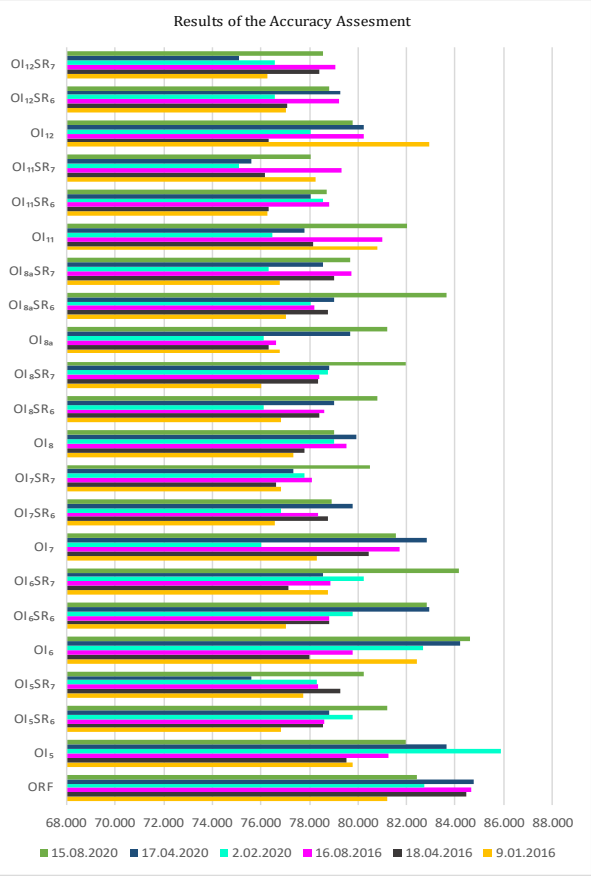

Figure 3. Accuracy Analysis Results

-In the changes obtained according to the combinations with the highest accuracy in 2016 and 2020 in the winter images (Figure 4 – Figure 5), it was observed that artificial green areas were formed because of the expropriation of the olive areas on the roadside. Therefore, it is understood that there has been a transformation from class O to class A. Technical errors in the classification of satellite data due to the ongoing construction of the Gemlik-Bursa North Interchange showed that U areas were confused with P class.

- Looking at the observations obtained from the spring images (Figure 6 – Figure 7), it is thought that there is a transformation from F areas to A areas, and that U and O classes have increased with the formation of rural settlements next to agricultural areas. It was also observed that the Gemlik-Bursa North Interchange, which was put into service on March 12, 2017, also affected the change of U areas.

- On the basis of the summer season (Figure 8 – Figure 9), it was concluded that the vegetation in the P class was mixed with the F class with the growing plant size.

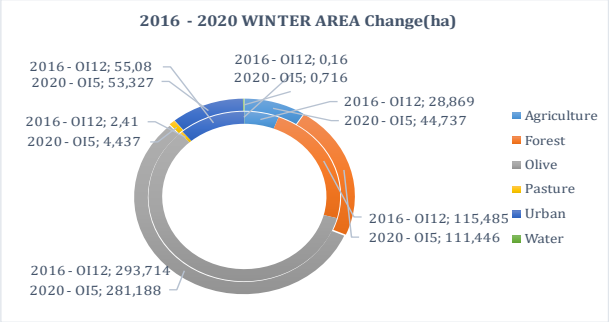

Figure 4. 2016 – 2020 the area changes in classes (Winter)

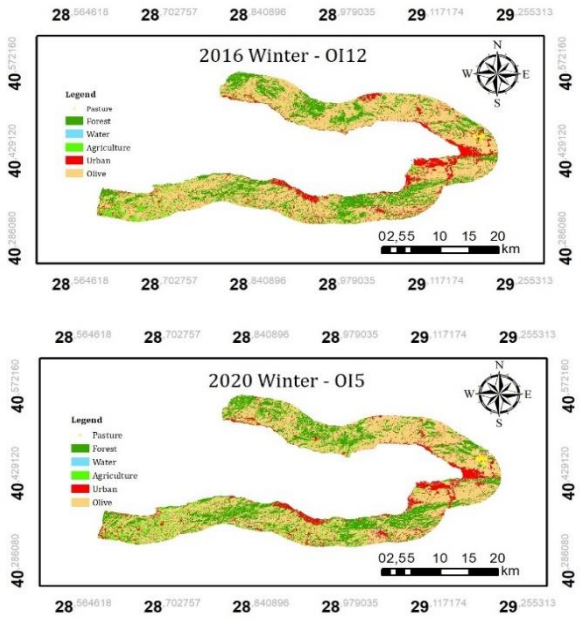

Figure 5. 2016 – 2020 the area changes in classes - map display (Winter)

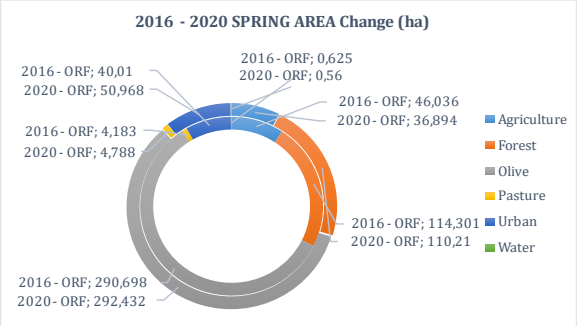

Figure 6. 2016 – 2020 the area changes in classes (Spring)

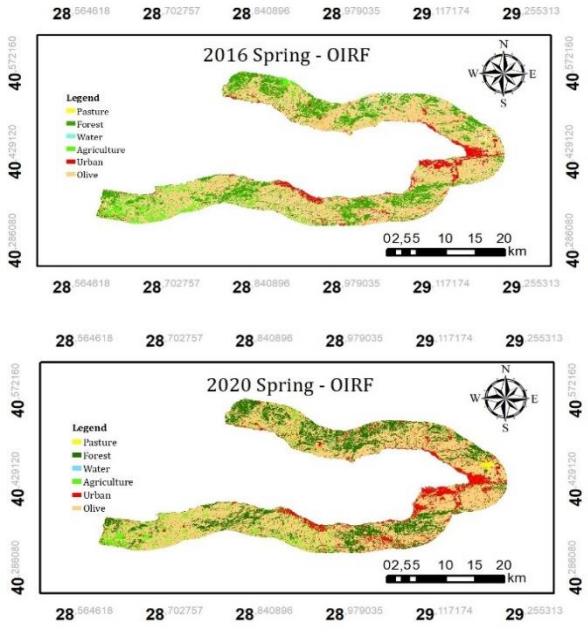

Figure 7. 2016 – 2020 the area changes in classes – map display (Spring)

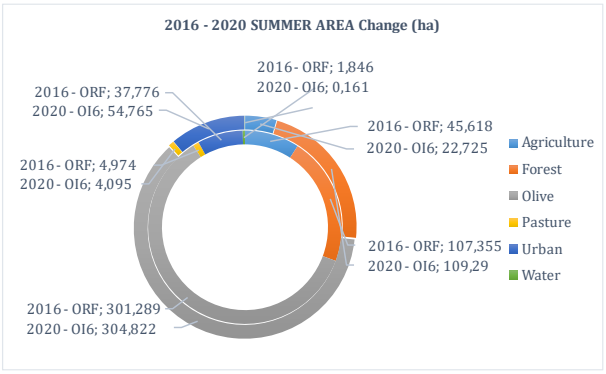

Figure 8. 2016 – 2020 the area changes in classes (Summer)

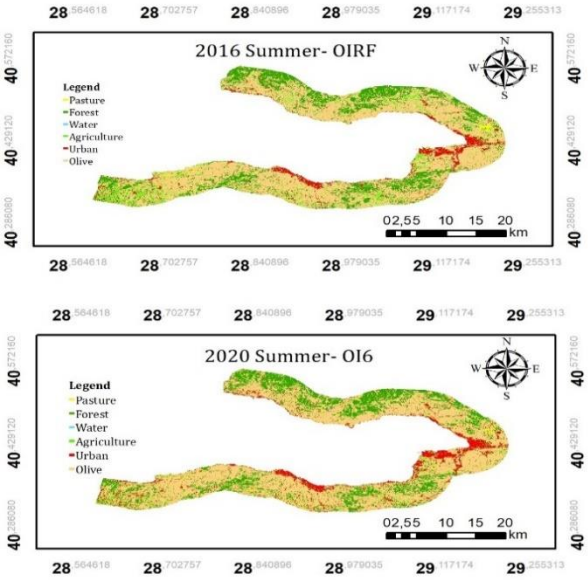

Figure 9. 2016 – 2020 the area changes in classes - map display (Summer)

4. DISCUSSION and CONCLUSION

4.1. Discussion

This study aimed to map LULC classes for three seasons using satellite imagery from 2016 and 2020 in order to observe the temporal effects of various state-funded investment decisions in Southeast Marmara region. It was found that the classification, using new indices, yielded accuracy results similar to those obtained from the original images. The construction of the TOGG factory and the decisions related to the Gemlik-Bursa Northern Interchange were observed to increase urbanization and consequently lead to population growth in the area. Additionally, it is believed that the COVID-19 pandemic, which occurred during the study period, led to an increase in the construction and real estate sectors, especially due to migrations to rural coastal areas such as Mudanya and Armutlu.

When examining the accuracy analysis results of the performed classifications, it was observed that the classification results from the original bands showed high accuracy. Additionally, the indices created using B6, B12, and B5 (indices without a simple ratio) also yielded favorable accuracy outcomes.

In this study, the combination that yielded the highest accuracy among index classifications was identified. The observed changes between 2016 and 2020 are believed to have resulted from various socioeconomic and technical reasons.

Accordingly, the dynamics of transformation from class O to class A in winter images are thought to be related to the expropriation of olive groves near the main road, leading to the creation of artificial green areas. Changes in classes U and P, on the other hand, were understood to be caused by technical errors in classification due to the continuation of the Gemlik-Bursa Northern Interchange project. In the spring season, there was a transformation from class F to class A due to the need for fertile soil. Consequently, the emergence of rural-urban areas, near agricultural areas led to an increase in classes U and O. Additionally, it was observed that the Gemlik-Bursa Northern Interchange, which became operational on March 12, 2017, impacted class U during the season. During the summer season, it was concluded that the growing vegetation height in class P often led to confusion with class F during the classification process. This study, conducted at the coastal scale, can be extended to examine other vegetation types in the region, and more detailed analyses can be applied.

The research emphasizes the importance of exploring the dynamics of land cover changes using new derived indices. In a study by Gitelson et al. (2002), various indices such as NDVI, ARVI, Soil Adjusted Vegetation Index (SAVI), and the red edge (700 nm) vegetation index were used for classification to measure sensitivity to atmospheric effects. It was found that NDVI yielded higher results. This study is in line with the aim of finding an index suitable for the purpose, but using existing indices may not provide a sufficient foundation for future modelling based on the accuracy assessment results which do not significantly differ from what expected.

A similar study conducted in the Western Ghats of South India addressed the effects of the pandemic through LULC classes and applied classification processes to Sentinel-2A satellite imagery using the NDVI index between 2018 and 2021. The study concluded that the dynamics of vegetation and urbanization changed due to the pandemic (Sathian & Brema, 2023). The outputs of this study, suggesting that changes in vegetation were based on urbanization, align with the findings of our study.

This study aimed to contribute to the literature by addressing the existing issues and providing an original perspective through the creation of LULC class results using classified images based on indices. In this context, our classifications and results have shown that investments in industrial zones near coastal areas are likely to have various effects, including population growth, migration movements, and changes in vegetation dynamics. It was determined that the increase in urban areas due to population growth had significant effects on LULC classes. The use of remote sensing data, different classification techniques, and various specific band combinations is expected to give more accurate results for future studies determining LULC dynamics.

4.2. Conclusion

The study was conducted to investigate LULC and vegetation dynamics along the coastal area of Southeastern Marmara Region with band combinations created using new vegetation indices. The combination that gives the best classification accuracy according to the seasons was determined and the accuracy analysis was used as a classification success scale. it was identified that how investment decisions taken by the government have led to an increase in impervious surfaces and how this has led to a change in other LULC classes The RF classification technique was applied to indices obtained from Sentinel-2A satellite images in three different seasons in 2016 and 2020. Subsequently, accuracy analysis was performed on classified images using ground control points obtained through Google Earth Pro. The study shows that the coastal area of Southeastern Marmara has been examined in detail with respect to LULC classes affected by various decisions using indices obtained from open-access and medium-resolution satellites. The study concludes that government investments in coastlines have caused significant LULC changes in the region and that these changes will be the beginning of other changes in the region. It is also concluded that the detailed LULC change detection can be further improved with the help of remote sensing and advance machine learning techniques.

In future studies, the use of machine learning methods, high-resolution images, more complex indices, and different classification techniques will facilitate a faster understanding of LULC dynamics and the investigation of future predictions.

Acknowledment

This study is part of the Eda ASCI's Master Thesis on Graduate School of Çanakkale Onsekiz Mart University, School of Graduate Studies, Department of Geographical Information Technology, Turkey.

Author contributions

E. Asci: Collected the datasets and analyzed the data, Classification, Validation.
L. Genc: Designed the research, Investigation, Writing the manuscript–review and editing.

Conflicts of Interest

The authors declare no conflict of interest.

Research and publication ethics statement

In the study, the authors declare that there is no violation of research and publication ethics and that the study does not require ethics committee approval.

REFERENCES

Ahamed, T., Tian, L., Zhang, Y. & Ting, K. C. (2011). A Review of Remote Sensing Methods for Biomass Feedstock Production. Biomass and Bioenergy, 35. https://doi.org/10.1016/j.biombioe.2011.02.028

Akturk, E. & Altunel, A. O. (2019). Accuracy Assesment of a Low-Cost UAV Derived Digital Elevation Model (DEM) in a Highly Broken and Vegetated Terrain. *Measurement,* 136, 382-386. https://doi.org/10.1016/j.measurement.2018.12.101

Asci, E., Inalpulat, M. & Genc, L. (2021). Identification of Residential Development Impacts on Agrıcultural Lands Using Landsat Imageries: Case Study of Bursa, Nilufer (1990-2020). *III. Balkan Agricultural Congress (AGRIBALKAN),* Edirne, Turkey.

Baeza, S. & Paruelo, J. M. (2020). Land Use/Land Cover Change (2000-2014) in The Rio De La Plata Grasslands: An Analysis Based on MODIS NDVI Time Series. *Remote Sensing*, 12(3). https://doi.org/10.3390/rs12030381

Barnes, E. M., Clarke, T. R., Richards, S. E., Colaizzi, P. D., Haberland, J., Kostrzewski, M., Waller , P., Choi, C., Rilye, E., Thomson, T., Lascano, R. J., Li, H. & Moran, M. S. (2000). Coincident Detection of Crop Water Stress, Nitrogen Status and Canopy Density Using Ground Based Multispectral Data. Proc. *5th Int. Conf. Precis Agric*, 1619(6).

Batunacun, Nendel, C., Hu, Y. & Lakes, T. (2018). Land-Use Changea and Land Degradation on The Mongolian Plateau from 1975 To 2015—A Case Study From Xilingol, China. *Land Degradation and Development,* 29(6), 1595–1606. https://doi.org/10.1002/LDR.2948

Breiman, L. (2001). Random Forests. *Machine Learning*, 45, 5-32. https://doi.org/10.1023/A:1010933404324

Cavur, M., Duzgun, H. S., Kemec, S. & Demirkan, D. C. (2019). Land Use and Land Cover Classification of Sentinel-2A: St.Petersburg Case Study. *International Archives of the Photogrammetry, Remote Sensing and Spatial Information Sciences - ISPRS Archives*, 42(1/W2). https://doi.org/10.5194/isprs-archives-XLII-1-W2-13-2019

Chan, J. C. W. & Paelinckx, D. (2008). Evaluation of Random Forest and Adaboost Tree-Based Ensemble Classification and Spectral Band Selection for Ecotope Mapping Using Airborne Hyperspectral Imagery. *Remote Sensing of Environment,* 112(6), 2999–3011. https://doi.org/10.1016/J.RSE.2008.02.011

Chandra Pandey, P., Koutsias, N., Petropoulos, G. P., Srivastava, P. K., & Ben Dor, E. (2019). Land Use/Land Cover in View of Earth Observation: Data Sources, Input Dimensions, and Classifiers-A Review of The State of The Art. *Geocarto International,* 36, 957–988. https://doi.org/10.1080/10106049.2019.1629647

Chehata, N., Guo, L. & Forests, R. (2009). Airborne Lidar Feature Selection for Urban Classification Using Random Forests. *Laser Scanning*, XXXVIII(3/W8), Paris, France.

Colkesen, I., Ozturk, M. Y., Kavzoglu, T. & Sefercik, U. G. (2021). Determination of sea surface mucilage formations using multitemporal Sentinel-2 imagery. *In Proceedings of the the 42nd Asian Conference on Remote Sensing (ACRS2021),* Can Tho City, Vietnam, 22-24.

Demarchi, L., Canters, F., Cariou, C., Licciardi, G. & Chan, J. C. W. (2014). Assessing The Performance of Two Unsupervised Dimensionality Reduction Techniques on Hyperspectral APEX Data for High Resolution Urban Land-Cover Mapping. *ISPRS Journal of Photogrammetry and Remote Sensing,* 87. https://doi.org/10.1016/j.isprsjprs.2013.10.012

Dewidar, K. M. (2010). Detection of Land Use/Land Cover Changes for the Northern Part of The Nile Delta (Burullus Region), Egypt. *International Journal of Remote Sensing,* 25(20), 4079–4089. https://doi.org/10.1080/01431160410001688312

El-naggar, A. M. (2018). Determination of optimum segmentation parameter values for extracting building from remote sensing images. *Alexandria engineering journal*, 57(4), 3089-

3097. https://doi.org/10.1016/j.aej.2018.10.001

Genc, L. (2002). Comparison of Landsat MSS and TM imagery for long term forest land cover change assessment. *Doctoral Thesis*, University of Florida, USA, 177p (in English).

Ghimire, B., Rogan, J., & Miller, J. (2010). Contextual Land-Cover Classification: Incorporating Spatial Dependence in Land-Cover Classification Models Using Random Forests and The Getis Statistic. *Remote Sensing Letters*, 1(1), 45–54. https://doi.org/10.1080/01431160903252327

Gitelson, A. A., Kaufman, Y. J., Stark, R. & Rundquist, D. (2002). Novel Algorithms for Remote Estimation of Vegetation Fraction. *Remote Sensing of Environment,* 80(1). https://doi.org/10.1016/S0034-4257(01)00289-9

Goel, E. & Abhilasha, E. (2017). Random Forest: A Review. *International Journal of Advanced Research in Computer Science and Software Engineering.* https://doi.org/10.23956/ijarcsse/v7i1/01113

Guan, H., Yu, J., Li, J. & Luo, L. (2012). Random Forests-Based Feature Selection For Land-Use Classification Using Lidar Data and Orthoimagery. *The International Archives of the Photogrammetry, Remote Sensing and Spatial Information Sciences,* XXXIX-B7. https://doi.org/10.5194/isprsarchives-xxxix-b7-203-2012

Herrmann, I., Pimstein, A., Karnieli, A., Cohen, Y., Alchanatis, V. & Bonfil, D. J. (2011). LAI Assessment of Wheat and Potato Crops by Venμs and Sentinel-2 Bands. *Remote Sensing of Environment,* 115(8). https://doi.org/10.1016/j.rse.2011.04.018

Hütt, C., Koppe, W., Miao, Y. & Bareth, G. (2016). Best Accuracy Land Use/Land Cover (LULC) Classification To Derive Crop Types Using Multitemporal, Multisensor, and Multi-Polarization SAR Satellite Images. *Remote Sensing.* https://doi.org/10.3390/rs8080684

Jamali, A. & Abdul Rahman, A. (2019a). Evaluation of Advanced Data Mining Algorithms in Land Use/Land Cover Mapping. *International Archives of the Photogrammetry, Remote Sensing and Spatial Information Sciences - ISPRS Archives,* 42(4/W16). https://doi.org/10.5194/isprs-archives-XLII-4-W16-283-2019

Jamali, A. & Abdul Rahman, A. (2019b). Sentinel-1 Image Classification For City Extraction Based on The Support Vector Machine and Random Forest Algorithms. *International Archives of the Photogrammetry, Remote Sensing and Spatial Information Sciences - ISPRS Archives*, 42(4/W16). https://doi.org/10.5194/isprs-archives-XLII-4-W16-297-2019

Joshi, R. R., Warthe, M., Dwivedi, S., Vijay, R. & Chakrabarti, T. (2011). Monitoring Changes in Land Use Land Cover of Yamuna Riverbed in Delhi: A Multi-Temporal Analysis. *International Journal of Remote Sensing*, 32(24), 9547–9558. https://doi.org/10.1080/01431161.2011.565377

Radhika, K. & Varadar, S. (2016). A Tutorial on Classification of Remote Sensing Data. *International Research Journal of Engineering and Technology (IRJET),* 3(8), 881-885.

Kavzoglu, T., Colkesen, I. & Yomralioglu, T. (2015). Object-Based Classification with Rotation Forest Ensemble Learning Algorithm Using Very-High-Resolution Worldview-2 Image. *Remote Sensing Letters,* 6(11). https://doi.org/10.1080/2150704X.2015.1084550

Kumar, V. & Agrawal, S. (2019). Agricultural Land Use Change Analysis Using Remote Sensing And GIS: A Case Study of Allahabad, India. *International Archives of the Photogrammetry, Remote Sensing and Spatial Information Sciences - ISPRS Archives*, 42(3/W6), 397–402. https://doi.org/10.5194/ISPRS-ARCHIVES-XLII-3-W6-397-2019

Le Maire, G., François, C. & Dufrêne, E. (2004). Towards Universal Broad Leaf Chlorophyll Indices Using PROSPECT Simulated Database and Hyperspectral Reflectance Measurements. *Remote Sensing of Environment,* 89(1). https://doi.org/10.1016/j.rse.2003.09.004

Main, R., Cho, M. A., Mathieu, R., O'Kennedy, M. M., Ramoelo, A. & Koch, S. (2011). An Investigation Into Robust Spectral Indices for Leaf Chlorophyll Estimation. *ISPRS Journal of Photogrammetry and Remote Sensing,* 66(6). https://doi.org/10.1016/j.isprsjprs.2011.08.001

Meinel, G. & Neubert, M. (2004). A Comparison of Segmentation Programs for High Resolution Remote Sensing Data*. International Archives of Photogrammetry and Remote Sensing,* 35(Part B), 1097-1105.

Mendoza, G. A. & Martins, H. (2006). Multi-Criteria Decision Analysis in Natural Resource Management: A Critical Review of Methods and New Modelling Paradigms. *Forest Ecology and Management,* 230, 1–22. https://doi.org/10.1016/j.foreco.2006.03.023

Mukhawana, M. B., Kanyerere, T. & Kahler, D. (2023). Review of In-Situ and Remote Sensing-Based Indices and Their Applicability for Integrated Drought Monitoring in South Africa. *Water*, 15. https://doi.org/10.3390/w15020240

Myint Htun, A., Shamsuzzoha, M. & Ahamed, T. (2023). Rice Yield Prediction Model Using Normalized Vegetation and Water Indices from Sentinel-2A Satellite Imagery Datasets. *Asia-Pacific Journal of Regional Science*, 7, 491–519. https://doi.org/10.1007/s41685-023-00299-2

Pal, M. (2005). Random Forest Classifier for Remote Sensing Classification. *International Journal of Remote Sensing,* 26(1), 217–222. https://doi.org/10.1080/01431160412331269698

Panigrahy, R. K., Ray, S. S. & Panigrahy, S. (2009). Study on the utility of IRS-P6 AWIFS SWIR band for crop discrimination and classification. *Journal of the Indian Society of Remote Sensing*, 37, 325-333. https://doi.org/10.1007/s12524-009-0026-6

Penuelas, J., Pinol, J., Ogaya, R., Filella, I., Pen Ä Uelas, J., Pin, J. & Ol, Ä. (1997). Estimation of Plant Water Concentration By The Reflectance Water Index WI (R900/R970). *International Journal of Remote Sensing,* 18(13), 2869–2875. https://doi.org/10.1080/014311697217396

Perumal, K. & Bhaskaran, R. (2010). Supervised Classification Performance of Multispectral Images. *Journal of Computing*, 2(2), 124-129.

Phiri, D., Simwanda, M., Salekin, S., Nyirenda, V. R., Murayama, Y. & Ranagalage, M. (2020). Sentinel-2 Data for Land Cover/Use Mapping: A Review. *Remote Sensing,* 12(14). https://doi.org/10.3390/rs12142291

Rodriguez-Galiano, V. F., Ghimire, B., Rogan, J., Chica-Olmo, M. & Rigol-Sanchez, J. P. (2012). An Assessment Of The Effectiveness Of A Random Forest Classifier For Land-Cover Classification. *ISPRS Journal of Photogrammetry and Remote Sensing,* 67(1), 93–104. https://doi.org/10.1016/J.ISPRSJPRS.2011.11.002

Sathian, S. & Brema, J. (2023). Assessment of Vegetative Cover Dynamics During Pre and Post Covid-19 Period Using Sentinel-2A Imageries in the Western Ghats, South India. *Journal of Metrology Society of India*, 14. https://doi.org/10.1007/s12647-023-00683-5

Scornet, E. (2015). Random Forests and Kernel Methods. *IEEE Transactions on Information Theory,* 62(3), 1485-1500. https://doi.org/10.1109/TIT.2016.2514489

Sharma, R. & Joshi, P. K. (2016). Mapping Environmental Impacts Of Rapid Urbanization in The National Capital Region of India Using Remote Sensing Inputs. *Urban Climate*, 15(2016), 70-82. https://doi.org/10.1016/j.uclim.2016.01.004

Tesfaye, A. A. & Gessesse Awoke, B. (2021). Evaluation of The Saturation Property of Vegetation Indices Derived from Sentinel-2 in Mixed Crop-Forest Ecosystem. Spatial Information Research, 29, 109-121. https://doi.org/10.1007/s41324-020-00339-5

Tucker, C. J. (1979). Red and Photographic Infrared Linear Combinations for Monitoring Vegetation. *Remote Sensıng of Environment*, 8, 127–150. https://doi.org/10.1016/0034-4257(79)90013-0

Tucker, C. J. (1980). Remote Sensing of Leaf Water Content in the Near İnfrared. *Remote Sensing of Environment,* 10(1), 23–32. https://doi.org/10.1016/0034-4257(80)90096-6

Whiteside, T. G., Boggs, G. S. & Maier, S. W. (2011). Comparing Object-Based and Pixel-Based Classifications for Mapping Savannas. *International Journal of Applied Earth Observation and Geoinformation*, 13(6), 884–893. https://doi.org/10.1016/j.jag.2011.06.008

Wu, C., Niu, Z., Tang, Q. & Huang, W. (2008). Estimating Chlorophyll Content from Hyperspectral Vegetation Indices: Modeling and Validation. *Agricultural and Forest Meteorology,* 148(8–9). https://doi.org/10.1016/j.agrformet.2008.03.005

Wu, T., Luo, J., Gao, L., Sun, Y., Dong, W., Zhou, N., Liu, W., Hu, X., Xi, J., Wang, C. & Yang, Y. (2021). Geo-Object-Based Vegetation Mapping via Machine Learning Methods with an Intelligent Sample Collection Scheme: A Case Study of Taibai Mountain, China. *Remote Sensing.* https://doi.org/10.3390/rs13020249

Xianju, L., Gang, C., Jingyi, L., Weitao, C., Xinwen, C. & Yiwei, L. (2017). Effects of RapidEye Imagery's Red-edge Band and Vegetation Indices on Land Cover Classification in an Arid Region. *Chinese Geographical Science,* 27(5), 827–835. https://doi.org/10.1007/s11769-017-0894-6

Yulianti, E. (2019). Multi-Temporal Sentinel-2 Images for Classification Accuracy. *Journal of Computer Science,* 15, 258–268. https://doi.org/10.3844/jcssp.2019.258.268

Zaidi, S. M., Akbari, A., Abu Samah, A., Kong, N. S. Gisen, J. I. A. (2017). Landsat-5 Time Series Analysis for Land Use/Land Cover Change Detection Using NDVI and Semi-Supervised Classification Techniques. *Polish Journal of Environmental Studies,* 26(6), 2833-2840. https://doi.org/10.15244/pjoes/68878

Zarco-Tejada, P. J., Miller, J. R., Noland, T. L., Mohammed, G. H. & Sampson, P. H. (2001). Scaling-Up and Model Inversion Methods with Narrowband Optical Indices for Chlorophyll Content Estimation in Closed Forest Canopies with Hyperspectral Data. *IEEE Transactions on Geoscience and Remote Sensing*, 39(7). https://doi.org/10.1109/36.934080

Zhang, T., Su, J., Liu, C., Chen, W. H., Liu, H., & Liu, G. (2017). Band selection in sentinel-2 satellite for agriculture applications. *In 2017 23rd international conference on automation and computing (ICAC)*, Huddersfield, UK, 1-6.